The Aeronautical Journal (2025), **129**, pp. 939–959
doi:10.1017/aer.2024.115

ROYAL AERONAUTICAL SOCIETY

RESEARCH ARTICLE

Research on multiple quadrotor UAV formation obstacle avoidance based on finite-time consensus

L. Zhang[1], R. Liu[1], B. Qu[1], T. Wei[2], X. Chai[1] and L. Yan[1]

[1]School of Automation and Electrical Engineering, Zhongyuan University of Technology, Zhengzhou, China
[2]School of Software, Henan University of Engineering, Zhengzhou, China
Corresponding authors: L. Zhang, B. Qu; Emails: 271274106@qq.com, quboyang@zut.edu.cn

Received: 21 February 2024; **Revised:** 13 August 2024; **Accepted:** 29 September 2024

Keywords: formation control; leader-following method; artificial potential field method; finite-time consensus

Abstract

Aiming at the problem of fast and consensus obstacle avoidance of multiple unmanned aerial systems in undirected network, a multi-quadrotor unmanned aerial vehicles UAVs (QUAVs) finite-time consensus obstacle avoidance algorithm is proposed. In this paper, multi-QUAVs establish communication through the leader-following method, and the formation is led by the leader to fly to the target position automatically and avoid obstacles autonomously through the improved artificial potential field method. The finite-time consensus protocol controls multi-QUAVs to form a desired formation quickly, considering the existence of communication and input delay, and rigorously proves the convergence of the proposed protocol. A trajectory segmentation strategy is added to the improved artificial potential field method to reduce trajectory loss and improve the task execution efficiency. The simulation results show that multi-QUAVs can be assembled to form the desired formation quickly, and the QUAV formation can avoid obstacles and maintain the formation unchanged while avoiding obstacles.

Nomenclature

UAV	Unmanned Aerial Vehicle
QUAV	Quadrotor Unmanned Aerial Vehicle

1.0 Introduction

Unmanned aerial vehicles (UAVs) have the advantages of low cost, high manoeuverability,and ease of operation [1–4]. When a single UAV completes complex tasks, its application is increasingly limited due to insufficient payload and sensor performance. Instead, more and more UAVs are working together to complete tasks, and the application and research of UAVs are beginning to develop towards clusters. UAV formation can perform tasks such as border patrol, battlefield reconnaissance, pesticide spraying and forest fire detection [5–8], which are widely used in both military and civil fields. Therefore, studying the problem of multi-UAV formation has important practical application value.

Categorised by the form of information exchange between individuals, multi-UAVs formation can be classified into centralised, distributed and decentralised structures [9]. In distributed control method, all agents act as independent control units and communicate information with neighbours to achieve state consistency control. Due to its better reliability and flexibility, this paper chooses the distributed control method. At present, the mainstream cluster formation control algorithms mainly include leader-following method [10], behaviour-based method [11], and virtual structure method [12]. Among them, the leader-following method is the most widely used, with the advantages of simple structure, easy implementation and wide applicability. The leader-following method is usually combined with the consistency method to design the formation algorithm [13].

Consistency method was first applied to the distributed control of communication network nodes. This method can enable the state of multiple nodes in communication network to reach a consistent state within a certain period of time. Due to its feasibility, this method is widely used in the control of multi-agent systems. Jadbabaie and Lin [14] applied knowledge of algebraic graph theory to theoretically prove that when the communication topology of the Vicsek model [15] is an undirected connected graph, all agents in the system will converge to the same state eventually. Olfati-Saber [16] studied the consensus problem of second-order continuous multi- agent system, extended the concept of algebraic connectivity in undirected graphs to directed graphs, and elucidated the important role of equilibrium directed graphs in solving the average consensus problem. Ni [17] studied the second-order multi-agent consensus problem under switching topology and proved that when the concatenation set of all the communicating topologies contains the minimum generation, the system will converge to consensus eventually.

The artificial potential field method is a distance-dominated method [18]. This method has the advantages of short computation time, real-time control, and safe and smooth planned trajectory. However, it also has disadvantages such as collision with obstacles, unreachable target and falling into local minimum. For these problems, many scholars have improved the artificial potential field method. Lawrence [19] provided general a technique for constructing guidance fields for UAV, which combines Lyapunov stability properties to generate simple, globally stable vector fields in 3D. Goncalves [20] proposed a method for computing artificial vector fields, which allows a UAV to converge to a specified general curve in n-dimensional space and loop around it. Wilhelm [21] focused on the optimisation of a gradient vector field UAV trajectory following and obstacle avoidance method, which minimise the deviation from an original trajectory. Hung [22] conducted an in-depth review of trajectory following control strategies applicable to a wide range class of marine, ground, and aerial autonomous robotic vehicles.

UAV formation obstacle avoidance not only requires avoiding obstacles, but also ensuring a safe distance between each UAV and inter-UAV communication. Due to various reasons such as communication links and devices, the network often experiences communication and input delay during the actual communication processes [23]. Therefore, the design and analysis of consistency method for multi-UAVs with time delay is more relevant.

The traditional consistency control can make the system state converge to the expected value when the time is infinite, but the finite-time consensus control can make the system state converge to the expected value within a finite time. Control algorithm in finite-time is proposed in Ref. (24). Adbessameud and Rtayebi [25] established a formation protocol with time delay for a second-order dynamics model of a multi-UAV system, and proved the stability of the protocol based on Lyapunov-Krasovskii theory. Sun [26] studied the finite time consistency problem of multi-UAV systems with leaders under fixed and switched networks by applying graph theory and Lasalle invariance principle. Ma [27] proposed a new distributed control law to study the leader-following consensus problem for finite-time linear time-invariant multi-agent system by assigning different priorities to each agent in the system. Shang [28] studied a first-order multi- agent system and obtained sufficient conditions for the system to achieve finite-time consensus under an undirected stationary topology.

Based on the earlier discussion, this paper improves on the Ref. (29) and studies obstacle avoidance problem of QUAV formation with finite-time consensus and time delay.

The main innovations are as follows:

(1) The traditional finite-time consensus protocol is improved, and considered the existence of time delay to accelerate the convergence speed of the system.

(2) The traditional artificial potential field method is improved, and the problems of the traditional artificial potential field method is solved.

(3) The trajectory segmentation strategy is introduced to reduce the complexity of QUAV obstacle avoidance environment and improve the task execution efficiency.

The rest of the paper is organised as follows. In Section 2, graph theory is given. In Section 3, a mathematical model of a QUAV is established. In Section 4, an improved finite-time consistency method

https://doi.org/10.1017/aer.2024.115 Published online by Cambridge University Press

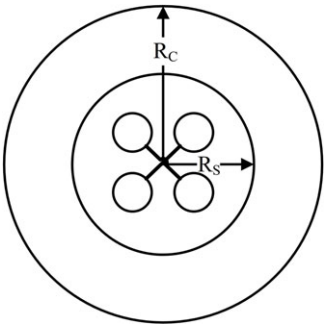

Figure 1. *Illustration of QUAV safety radius profile.*

is given with considered the existence of time delay. In Section 5, the improved artificial potential field method is introduced. In Section 6, a finite-time consensus formation obstacle avoidance algorithm with time delay is proposed based on the leader-following method. In Section 7, MATLAB simulation results are given. In Section 8, conclusion is given.

2.0 Graph theory

QUAV formation consensus control covers multiple aspects such as formation reconstruction, formation maintenance, obstacle avoidance and so on, all of which are designed based on graph theory. In graph theory, a graph is composed of vertexes and edges, where the vertexes represent the QUAVs and the edges represent the communication between the QUAVs.

Assuming the total number of QUAVs is n. The graph $G = (V, E)$ consists of a vertex set $V = (1, 2, \cdots, n)$ and an edge set $E \subseteq V \times V$. If vertex i and vertex j are connected, then there's an edge $(v_i, v_j) \in E$, and vertex j is called a neighbour of vertex i. Graphs are divided into directed graphs and undirected graphs, if all the edges in a graph are undirected, it is called an undirected graph; otherwise, it is called a directed graph.

The relationship between vertex i and vertex j is representedby a_{ij}. If vertex i and vertex j are connected by an edge, then $a_{ij} = 1$; otherwise, $a_{ij} = 0$. The adjacency matrix $A = [a_{ij}](i, j \in \{1, 2, \cdots, n\})$ is a method used in graph theory to represent a graph as a two-dimensional array, where the rows and columns represent the vertexes in the graph, and the elements of the array represent whether there are edges between the vertices.

The degree matrix $D = diag(d_1, d_2, \ldots, d_n)$ is diagonal arrays, and the elements on the diagonal represent the degrees of a single vertex. In an undirected graph, the degree $d(v_i)$ of a vertex is the number of edges of vertex i. In a directed graph, degree is divided into two concepts: in-degree and out-degree. The in-degree is the number of directed edges that end at the vertex; the out-degree is the number of directed edges starting from the vertex.

The Laplace matrix of a graph is related to the degree matrix and the adjacency matrix by $L = D - A$.

3.0 Mathematical models

The UAV model used in this paper is a QUAV, assuming that the safety radius of the centre of the QUAV is R_S and the communication radius is R_C. The distance between the centre of the QUAV and the surface of the obstacle needs to be greater than the safety radius; otherwise, a collision may occur, resulting in a crash. The distance between any two QUAV centres needs to be less than the communication radius; otherwise it will cause the QUAV to lose contact. The safety radius and communication radius are illustrated in Fig. 1.

https://doi.org/10.1017/aer.2024.115 Published online by Cambridge University Press

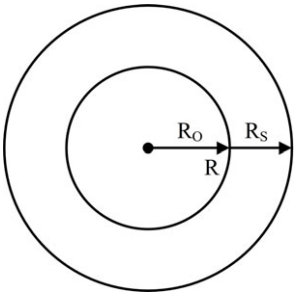

Figure 2. *Illustration of obstacle safety radius profile.*

The continuous-time multi-QUAVs linear model used in this paper is:

$$\dot{x}_i(t) = u_i(t), i \in N \tag{1}$$

where, $x_i(t) \in R$ and $u_i(t) \in R$ denote the state and control input of QUAV i at moment t, respectively.

Due to the fact that QUAV is a linear model, it is treated as a mass point in the artificial potential field method, which contradicts the safety radius that the QUAV needs to maintain. It is necessary to attach the safety radius of the QUAV to the obstacle, which the QUAV is treated as a mass point and no longer requires a safety radius. Assuming the actual radius of the spherical obstacle is R_O, the total radius $R = R_O + R_S$. The radius of the obstacle is shown in Fig. 2.

4.0 Finite-time consensus with time delay

The consensus protocol with equal communication delay, input delay and undirected connected graph network topology is as follows:

$$u_i(t) = \sum_{V_j \in N_i} a_{ij}\left(x_j(t-\tau) - x_i(t-\tau)\right) \tag{2}$$

where, τ denotes the time delay; when $\tau \in [0, \pi/2\lambda_n)$ the system can achieve consistent; λ_n is the maximum eigenvalue of the Laplace matrix of the system.

Definition 1 [30] If there exists an expected time $T_0 \in [0, +\infty)$, such that for any initial state, the multi-QUAVs satisfy $\lim_{t \to T_0} \|x_i(t) - x_0(t)\| = 0$ and $x_i(t) = x_0(t), \forall t \geqslant T_0, i \in I$, then it can be said that finite-time consensus control has been achieved.

In Ref. (31), Sun and Guan proposed the following finite-time consensus protocol:

$$u_i(t) = \sum_{j \in N_i} a_{ij} sig^{\alpha}\left(x_j(t) - x_i(t)\right) + a_{i0} sig^{\alpha}\left(x_0(t) - x_i(t)\right) \tag{3}$$

where $0 < \alpha < 1$.

Definition 2 $sig^{\alpha}(x_i) = |x_i|^{\alpha} \text{sgn}(x_i)$, sgn() is a symbolic function, defined as $sgn(r) = \begin{cases} 1, & r > 0 \\ 0, & r = 0 \\ -1, & r < 0 \end{cases}$.

Considering the existence of time delay based on protocol (3), protocol (4) is obtained:

$$u_i(t) = \sum_{j \in N_i} a_{ij} sig\left(x_j(t-\tau) - x_i(t-\tau)\right)^{\alpha} + a_{i0} sig\left(x_0(t-\tau) - x_i(t-\tau)\right)^{\alpha} \tag{4}$$

In order to accelerate the convergence speed of protocol (4), this paper has made improvements and proposed protocol (5):

https://doi.org/10.1017/aer.2024.115 Published online by Cambridge University Press

$$u_i(t) = \sum_{j\in N_i} a_{ij} sig\left(x_j(t-\tau) - x_i(t-\tau)\right)^{\alpha} + a_{i0} sig\left(x_0(t-\tau) - x_i(t-\tau)\right)^{\alpha} \\ + \beta \sum_{j\in N_i} a_{ij}\left(x_j(t-\tau) - x_i(t-\tau)\right) + \beta a_{i0}\left(x_0(t-\tau) - x_i(t-\tau)\right) \tag{5}$$

where, $\beta > 0$, the larger β is, the faster system converges.

Next, it will be proven that protocol (5) can achieve finite-time consensus and has a faster convergence speed than protocol (4). Before that, the following lemmas need to be introduced.

Lemma 1: [32] *Suppose that the function* $\varphi : R^2 \to R$ *satisfies the condition* $\varphi\left(x_i, x_j\right) = -\varphi\left(x_j, x_i\right)$, $\forall i, j \in I, i \neq j$, *and then* $\sum_{i=1}^{N}\sum_{j\in N_i} a_{ij} y_i \varphi\left(x_j, x_i\right) = -\frac{1}{2}\sum_{(v_i,v_j)\in E} a_{ij}\left(y_j - y_i\right)\varphi\left(x_j, x_i\right)$ *is satisfied for any undirected graph and series* $y_1, y_2, \ldots, y_n$.

Lemma 2: [33] *If* $y_1, y_2, \ldots, y_n > 0$ *and* $0 < p \leq 1$, *then* $\sum_{i=1}^{n} y_i^p \geqslant \left(\sum_{i=1}^{n} y_i\right)^p$.

Lemma 3: (34) $L(A) = \left[l_{ij}\right] \in R^{n\times n}$ ***denotes the Laplace matrix of graph*** $G(A)$***, which has the following properties:***

(1) $x^T L(A)x = \frac{1}{2}\sum_{i,j=1}^{n} a_{ij}\left(x_j - x_i\right)^2$, *the semi positive characterisation of* $L(A)$ *indicates that all its eigenvalues are real numbers and not less than zero.*

(2) If the graph $G(A)$ *is connected, the second smallest eigenvalue of* $L(A)$ *is greater than zero, denoted by* $\lambda_2\ (L_A)$, *which is called as the algebraic connectivity of the graph* $G(A)$.

(3) The algebraic connectivity of the graph $G(A)$ *is equal to* $\min_{x\neq 0_n, 1_n^T x=0} x^T L(A)x / x^T x$, *and if* $1_n^T x = 0$, *then* $x^T L(A)x \geqslant \lambda_2\ (L_A)\ x^T x$.

(4) If graph $G(A)$ *is an undirected connected graph, then* $L(A) + Diag\ (b_1, \ldots, b_n)$ *is positive definite, where* $b_i \geqslant 0$, $\forall i \in I$ *and there exists at least one* $b_i > 0$.

Lemma 4: [35] *Consider the non-Lipschitz continuous nonlinear systems* $\dot{x} = f(x)$ *and* $f(0) = 0$, *suppose there is a differential function* $V(x)$ *defined in the neighbourhood of the origin, and there exist* $c > 0$ *and* $0 < \alpha < 1$ *such that* $V(x)$ *is positive definite and* $\dot{V}(x) + cV^{\alpha} \leq 0$, *and then the origin is considered locally finite-time stable. The finite-time* T*depends on the initial state* x_0, *and satisfy* $T(x_0) \leq V(x_0)^{1-\alpha}/c(1-\alpha)$.

Next, using the Lyapunov function method, it is shown that the control of multi-QUAVs through protocol (5) can achieve state consensus within a finite-time.

Proof: Define the position error

$$e_i(t) = x_i(t-\tau) - x_0(t-\tau), \quad \forall i \in I \tag{6}$$

This is obtained through Equations (1) and (6):

$$\dot{e}_i(t) = \sum_{j\in N_i} a_{ij} sig\left(e_j(t) - e_i(t)\right)^{\alpha} - a_{i0} sig(e_i(t))^{\alpha} + \beta \sum_{j\in N_i} a_{ij}\left(e_j(t) - e_i(t)\right) - \beta a_{i0} e_i(t) \tag{7}$$

$$= \sum_{j=0}^{n} a_{ij} sig\left(e_j(t) - e_i(t)\right)^{\alpha} + \beta \sum_{j=0}^{n} a_{ij}\left(e_j(t) - e_i(t)\right)$$

https://doi.org/10.1017/aer.2024.115 Published online by Cambridge University Press

The Lyapunov function $V_1(t) = \sum_{i=0}^{n} e_i^2(t)$ chosen according to Lemma 1 is given by Equation (7):

$$\begin{aligned}
\dot{V}_1(t) &= 2\sum_{i=0}^{n} e_i(t)\dot{e}_i(t) \\
&= 2\sum_{i=0}^{n} e_i(t)\left[\sum_{j=0}^{n} a_{ij} sig\left(e_j(t)-e_i(t)\right)^{\alpha} + \beta\sum_{j=0}^{n} a_{ij}\left(e_j(t)-e_i(t)\right)\right] \\
&= 2\sum_{i=0}^{n} e_i(t)\sum_{j=0}^{n} a_{ij} sig\left(e_j(t)-e_i(t)\right)^{\alpha} + 2\beta\sum_{i=0}^{n} e_i(t)\sum_{j=0}^{n} a_{ij}\left(e_j(t)-e_i(t)\right) \\
&= -\sum_{i=0}^{n}\sum_{j=0}^{n} a_{ij} sig\left(e_j(t)-e_i(t)\right)^{\alpha}\left(e_j(t)-e_i(t)\right) - \beta\sum_{i=0}^{n}\sum_{j=0}^{n} a_{ij}\left(e_j(t)-e_i(t)\right)^2 \\
&= -\sum_{i=0}^{n}\sum_{j=0}^{n} a_{ij}\left(e_j(t)-e_i(t)\right)^{1+\alpha} - \beta\sum_{i=0}^{n}\sum_{j=0}^{n} a_{ij}\left(e_j(t)-e_i(t)\right)^2 \\
&< -\sum_{i=0}^{n}\sum_{j=0}^{n} a_{ij}\left(e_j(t)-e_i(t)\right)^{1+\alpha} \\
&= -\sum_{i=0}^{n}\sum_{j=0}^{n}\left[a_{ij}^{\frac{2}{1+\alpha}}\left(e_j(t)-e_i(t)\right)\right]^{\frac{1+\alpha}{2}}
\end{aligned} \tag{8}$$

From Lemma 2, it can be concluded that:

$$\dot{V}_1(t) \le -\left[\sum_{i=0}^{n}\left(\sum_{j=0}^{n} a_{ij}^{\frac{2}{1+\alpha}}\left(e_j(t)-e_i(t)\right)\right)^2\right]^{\frac{1+\alpha}{2}} \tag{9}$$

Let $B = L(A) + Diag(a_{10}, \ldots, a_{n0})$, from Lemma 3, we can conclude that:

$$\frac{\sum_{i=0}^{n}\left[\sum_{j=0}^{n} a_{ij}^{\frac{2}{1+\alpha}}\left(e_j(t)-e_i(t)\right)\right]^2}{V_1(t)} = \frac{2e_i^T(t)Be_i(t)}{e_i^T(t)e_i(t)} \geqslant 2\lambda_2\left(L_B\right) \tag{10}$$

Combining Equations (9) and (10) yields $\dot{V}_1(t) \le -[2\lambda_2(L_B)]^{\frac{1+\alpha}{2}} V(t)^{\frac{1+\alpha}{2}}$, and by Lemma 4 $T(x(0)) \le \frac{2V_1(0)^{\frac{1-\alpha}{2}}}{(1+\alpha)[2\lambda_2(L_B)]^{\frac{1+\alpha}{2}}}$. And that's the end of the proof.

In the following, by choosing the same Lyapunov function $V_2(t) = \sum_{i=0}^{n} e_i^2(t)$, it is shown that the convergence of the multi-QUAV formation under protocol (5) is faster than that under protocol (4) in the same way as described earlier.

$$\begin{aligned}
\dot{V}_2(t) &= 2\sum_{i=0}^{n} e_i(t)\dot{e}_i(t) \\
&= 2\sum_{i=0}^{n} e_i(t)\left[\sum_{j=0}^{n} a_{ij} sig\left(e_j(t)-e_i(t)\right)^{\alpha}\right]
\end{aligned}$$

https://doi.org/10.1017/aer.2024.115 Published online by Cambridge University Press

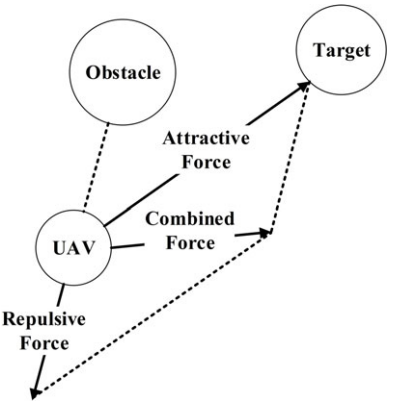

Figure 3. *Illustration of artificial potential field method.*

$$
\begin{aligned}
&= 2\sum_{i=0}^{n} e_i(t) \sum_{j=0}^{n} a_{ij} sig\big(e_j(t) - e_i(t)\big)^{\alpha} \\
&= -\sum_{i=0}^{n}\sum_{j=0}^{n} a_{ij} sig\big(e_j(t) - e_i(t)\big)^{\alpha} \big(e_j(t) - e_i(t)\big) \\
&= -\sum_{i=0}^{n}\sum_{j=0}^{n} a_{ij} \big(e_j(t) - e_i(t)\big)^{1+\alpha}
\end{aligned}
\tag{11}
$$

From Equation (8), we can obtain $\dot{V}_1(t) = -\sum_{i=0}^{n}\sum_{j=0}^{n} a_{ij}\big(e_j(t) - e_i(t)\big)^{1+\alpha} - \beta \sum_{i=0}^{n}\sum_{j=0}^{n} a_{ij}\big(e_j(t) - e_i(t)\big)^{2}$, and from $\beta > 0$ easily know $\dot{V}_2(t) < \dot{V}_1(t)$. Therefore, the convergence speed of protocol (5) is faster than that of protocol (4).

5.0 Artificial potential field method

5.1 Traditional artificial potential field method

The traditional artificial potential field method is created based on the principle of force in physics. It regards the controlled object as a particle and studies its motion in a virtual potential field. The QUAV moves towards the target position under the influence of potential field and avoids obstacles during this process. The whole potential field consists of two parts: gravitational potential field and repulsive potential field. By calculating the negative gradient of the gravitational potential field and repulsive potential field acting on the QUAV, gravity and repulsive force are obtained, where the force at the target point is gravity and the force at the obstacle is repulsive force. Under the combined action of gravity and repulsion, the QUAV can move toward the target point while avoiding obstacles, and a smooth and continuous motion trajectory can be generated during the whole movement process. The principle of artificial potential field method is shown in Fig. 3.

The traditional artificial potential field method has the following shortcomings [36]:

(1) Collision with obstacles. When the distance between the QUAV and the target point is too far, the attractive force on it will be much greater than the repulsive force, and it may collide with obstacles during flight.

(2) Target unreachability. When the target point is located near an obstacle and the QUAV approaches the target point, the repulsive force applied to the QUAV is too strong relative to the attractive force, causing the QUAV to hover or remain stationary in a certain area.

https://doi.org/10.1017/aer.2024.115 Published online by Cambridge University Press

(3) Falling into a local minimum. When the QUAV moves to a non-target point location, it will fall into a local minimum due to force equilibrium, causing it to oscillate or come to rest repeatedly near the local minimum point.

5.2 Improved artificial potential field method

The attractive potential field function is improved to address the problem of excessive attractive force caused by the QUAV being too far away from the target. Set the attraction action threshold for segment to avoid the problem of excessive attraction force. The modified attractive potential field function is shown in Equation (12):

$$U_{att}(q) = \begin{cases} \frac{1}{2}k_{att}{d_{goal}}^2, & d_{goal} \le d_0 \\ d_0 k_{att} d_{goal} - \frac{1}{2}k_{att}d_0^2, & d_{goal} > d_0 \end{cases} \tag{12}$$

where, k_{att} is the attractive coefficient, d_0 is the impact distance threshold of the target point, q is the spatial position of the QUAV, and $d_{goal} = \left\| q - q_{goal} \right\|_2$ is the Euclidean distance between the QUAV and the target point.

The attraction force is the negative gradient of the attractive potential field, as shown in Equation (13):

$$F_{att}(q) = -\nabla U_{att}(q) = \begin{cases} k_{att}\left(q_{goal} - q\right), & d_{goal} \le d_0 \\ \frac{d_0}{d_{goal}}k_{att}\left(q_{goal} - q\right), & d_{goal} > d_0 \end{cases} \tag{13}$$

For the target unreachability problem, an improved repulsive potential field function is introduced, which combines the distance between the target point and the QUAV to ensure that the potential field is globally minimised at the target point only. The improved repulsive potential field function is shown in Equation (14):

$$U_{rep}(q) = \begin{cases} \frac{1}{2}k_{rep}(\frac{1}{d_{obs}} - \frac{1}{d_{\max}})^2 d_{goal}^2, & d_{obs} \le d_{\max} \\ 0, & d_{obs} > d_{\max} \end{cases} \tag{14}$$

where, K_{rep} is the repulsive coefficient, d_0 is the maximum impact distance of an obstacle, and $d_{obs} = \|q - q_{obs}\|_2$ is the Euclidean distance between the QUAV and the obstacle.

The repulsive force is the negative gradient of the repulsive potential field, as shown in Equation (15):

$$F_{rep}(q) = -\nabla U_{rep}(q) = \begin{cases} F_{rep1}\mathbf{n}_1 + F_{rep2}\mathbf{n}_2, & d_{obs} \le d_{\max} \\ 0, & d_{obs} > d_{\max} \end{cases} \tag{15}$$

where, $\mathbf{n}_1$and $\mathbf{n}_2$ denote the unit direction vectors along the directions F_{rep1} and F_{rep2}. The expressions for F_{rep1} and F_{rep2} are shown in Equation (16):

$$\begin{cases} F_{rep1} = k_{rep}\left(\frac{1}{d_{obs}} - \frac{1}{d_{\max}}\right)\frac{d_{goal}^2}{d_{obs}^2} \\ F_{rep2} = \frac{n}{2}k_{rep}\left(\frac{1}{d_{obs}} - \frac{1}{d_{\max}}\right)^2 d_{goal} \end{cases} \tag{16}$$

where F_{rep1} and F_{rep2} are the components of the repulsive force in two different directions, respectively.

The direction of vector points from the obstacle to the QUAV, which is the repulsive force component; the direction of vector points from the QUAV to the target point and is the attractive force component. As shown in Fig. 4.

It is important to note that the QUAVs in the formation also need to avoid collisions with each other. QUAVs can consider each other as dynamic obstacles, obtain the positions of other QUAVs, and avoid collisions through artificial potential field methods.

https://doi.org/10.1017/aer.2024.115 Published online by Cambridge University Press

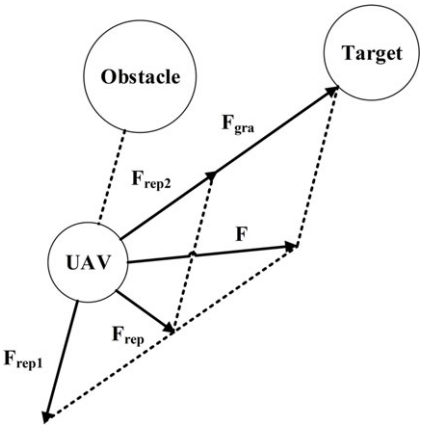

Figure 4. *Illustration of repulsive force calculation method.*

The total potential field consists of attractive potential field and repulsive potential field, as shown in Equation (17):

$$U(q) = U_{att}(q) + U_{rep}(q) \tag{17}$$

The combined force is equal to the negative gradient of the total potential field, as shown in Equation (18):

$$F(q) = -\nabla U(q) \tag{18}$$

For the local minimum problem, introduce a random perturbation and set the minimum velocity as the condition for triggering the random perturbation. If the velocity components v_x, v_y, v_z of the QUAV in all three directions of x, y, z are less than the minimum velocity, the random perturbation is triggered, as shown in Equation (19):

$$v_{rand} = \begin{bmatrix} v_x \\ v_y \\ v_z \end{bmatrix} = \begin{bmatrix} \lambda(2\text{rand} - 1) \\ \lambda(2\text{rand} - 1) \\ \lambda(2\text{rand} - 1) \end{bmatrix}, \quad v_x < v_{\min}\ v_y < v_{\min}\ v_z < v_{\min} \tag{19}$$

where, is a random function, is the minimum velocity, λ is a coefficient with a small absolute value, and 2rand is a random number in the range of 0 to 1.

5.3 Constraint conditions

In order to avoid collision between QUAVs and obstacles due to excessive speed, a maximum speed constraint is introduced and the constraints are v_x, v_y, v_z.

Taking the velocity component of the X-axis as an example,and calculate the velocity change at each sampling time, as shown in Equation (20):

$$\Delta v_x(t) = v_x(t) - v_x(t-1) \tag{20}$$

where, $v_x(t)$ is the speed of the QUAV at the current sampling time, $v_x(t-1)$ is the speed of the QUAV at the last sampling time, and $\Delta v_x(t)$ is the amount of change in the velocity component.

Then, the velocity component of the QUAV at the next sampling time is calculated, as shown in Equation (21):

https://doi.org/10.1017/aer.2024.115 Published online by Cambridge University Press

$$\begin{cases} v_{0x}(t+1) = \begin{cases} \min\{v(t)+\Delta v(t), v(t)+a_x \cdot dt\}, \Delta v(t) > 0 \\ \max\{v(t)+\Delta v(t), v(t)-a_x \cdot dt\}, \Delta v(t) < 0 \end{cases} \\ v_x(t+1) = \begin{cases} \min\{v_{0x}(t+1), +v_{x\max}\}, v_{0x}(t+1) > 0 \\ \max\{v_{0x}(t+1), -v_{x\max}\}, v_{0x}(t+1) < 0 \end{cases} \end{cases} \tag{21}$$

where, $v_{x\max}$ is the maximum velocity component of the QUAV, a_x is the acceleration component. The values of $v_{x\max}$ and a_x need to meet the requirement that the QUAV can avoid collision by decelerating when encountering obstacles. $v_{0x}(t+1)$ plays a transitional role in determining the $v_x(t+1)$ of the velocity component of the QUAV at the next sampling time.

5.4 Trajectory segmentation strategy

Collision detection and avoidance are important components of the trajectory strategy, and in environments with long total paths or many obstacles, the artificial potential field method has some randomness in trajectory planning, and the result may not be the optimal trajectory. This section improves the artificial potential field method by segmenting the total path to reduce the complexity of the obstacle environment.

The obstacles encountered by QUAVs during actual flight are mostly irregular three-dimensional objects. If the repulsive potential field is calculated at each trajectory point of the obstacle boundary points, it will result in a strategic trajectory with frequent turning and easy to oscillate, which does not satisfy the QUAV shortest trajectory segment constraint. For irregular concave and convex body obstacles, the general solution is to create a complete envelope of an outer jointed sphere for them and use the outer jointed sphere as a new obstacle to be avoided.

The following is an example of a spherical obstacle to introduce the calculation method of trajectory segmentation strategy:

(1) If the starting point S(x_S, y_S, z_S) and the ending point G(x_G, y_G, z_G) are known, draw a line L_{SG} through these two points. Let its direction vector be (d_x, d_y, d_z). The parametric equation of L_{SG} is given in Equation (22):

$$\begin{cases} x = x_S + d_x \cdot t \\ y = y_S + d_y \cdot t \\ z = z_S + d_z \cdot t \end{cases} \tag{22}$$

(2) Judgement whether the line L_{SG} intersects with an obstacle. If L_{SG} does not intersect with any obstacle, L_{SG} is the target trajectory; otherwise, judgement the spherical centre C$(x_C, y_C z_C)$ of the obstacle and its safe radius r_C that intersects with L_{SG} and is closest to the starting point. The spherical expression of the obstacle is shown in Equation (23):

$$(x - x_C)^2 + (y - y_C)^2 + (z - z_C)^2 = r_C^2 \tag{23}$$

(3) Find the value of the parameter t by combining Equations (22) and (23), and substitute it into Equation (22) to obtain the two intersection points A and B between the line and the sphere. Calculate the coordinates of the midpoint M of the line segment AB.

(4) Connect the centre of the sphere C and the point M to obtain the line L_{CM}. Calculate the other two intersections E and F of L_{CM} of the sphere in the same way as above.

(5) Calculate and compare the distances between point E and point F from the starting point S respectively. Use the point closer to the starting point S as the new target point.

(6) Execute the formation consensus obstacle avoidance algorithm, when the leader reaches a new target position, use this position as a new starting point. Repeat steps (1)–(5) to find the next new target point until the QUAV reaches the desired target point.

https://doi.org/10.1017/aer.2024.115 Published online by Cambridge University Press

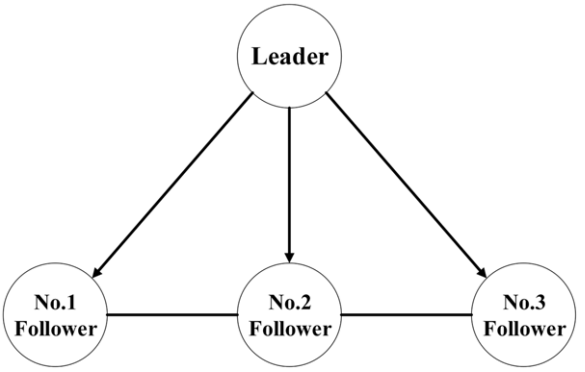

Figure 5. *Illustration of leader-following method.*

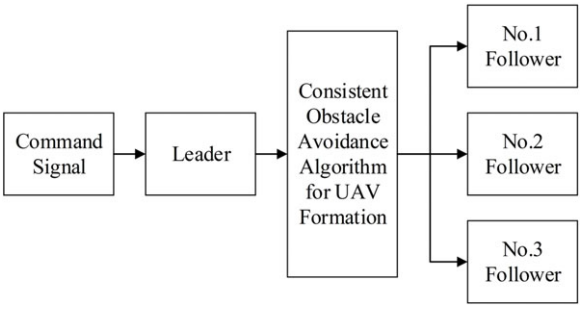

Figure 6. *Illustration of QUAV formation control structure.*

The trajectory segmentation strategy can reduce the complexity of the QUAV flight environment. By calculating the sub-target points, the planned trajectory is guaranteed to be the optimal solution, which reduces the flight cost and improves the task execution efficiency.

6.0 Mutli-quavs formation consensus obstacle avoidance algorithm

The formation control adopts the leader-following method in distributed control, and its basic idea is that: the leader receives commands and controls the entire formation to perform the expected task. The followers follow the leader based on their expected positions relative to the leader. The leader-following method is illustrated in Fig. 5:

The control protocol of the leader is shown in Equation (24):

$$u_0(t) = \sum_{i \in N_i} a_{i0} \Delta x_{i0}(t) + F_0(t) + v_{rand} \tag{24}$$

where $\Delta x_{i0}(t)$ is the relative position of the leader and the follower i at moment t, $F_0(t)$ is the combined force on the leader at moment t.

The control protocol of the follower is shown in Equation (25):

$$u_i(t) = \sum_{j \in N_i} a_{ij} \left(x_j(t-\tau) - x_i(t-\tau) - \Delta x_{ij}(t) \right) + F_{rep(i)}(t) \tag{25}$$

where $\Delta x_{ij}(t)$ denotes the relative position of QUAV i and QUAV j at moment t, and $F_{rep(i)}(t)$ the obstacle repulsive force on QUAV i at moment t.

https://doi.org/10.1017/aer.2024.115 Published online by Cambridge University Press

Table 1. *Position coordinates of six QUAVs*

Name	Initial position	Desired position
Follower 1	(2, 6, 0)	(−2, 0, 0)
Follower 2	(6, 2, 0)	(0, −2, 0)
Follower 3	(2, 4, 0)	(−4, 0, 0)
Follower 4	(2, 2, 0)	(−2, −2, 0)
Follower 5	(4, 2, 0)	(0, −4, 0)
Leader	(4, 4, 0)	(0, 0, 0)

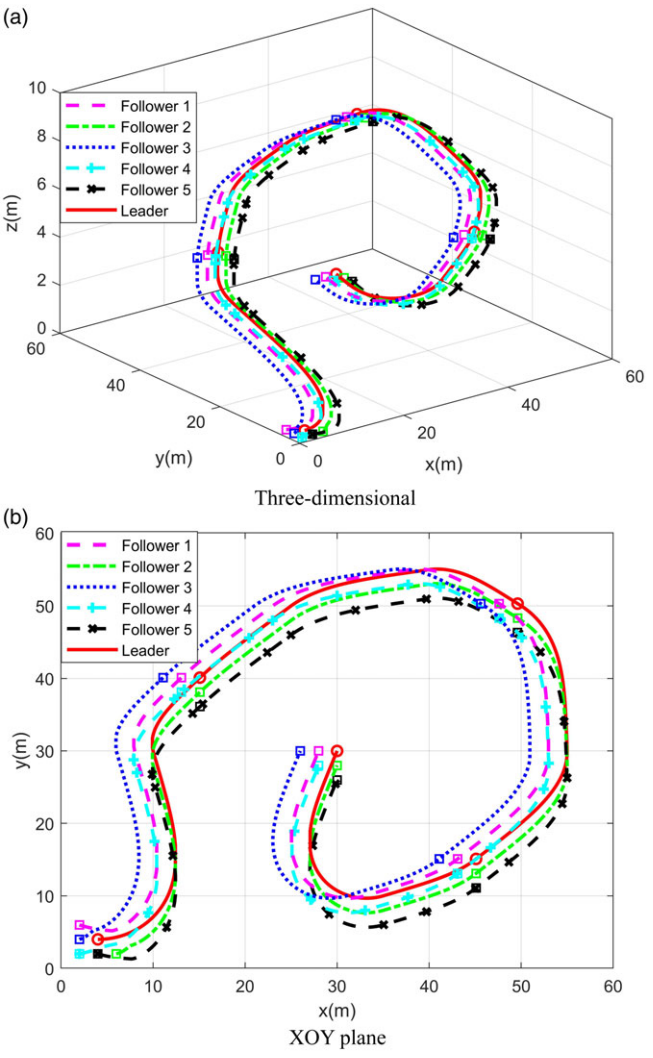

Figure 7. *Formation consensus of six QUAVs.*

After receiving the command signal, the leader QUAV sends control command to the followers through the formation consensus obstacle avoidance algorithm. The followers enter the range of influence of obstacles and avoid them autonomously, thus realising a consistent state throughout the formation. The QUAV formation control structure is shown in Fig. 6.

https://doi.org/10.1017/aer.2024.115 Published online by Cambridge University Press

Table 2. *Position coordinates of four QUAVs*

Name	Initial position	Desired position
Follower 1	(1, 2, 1)	(−2, 0, 0)
Follower 2	(1, 1, 0.7)	(−1, −1, 0)
Follower 3	(2, 1, 0.3)	(0, −2, 0)
Leader	(2, 2, 0)	(0, 0, 0)

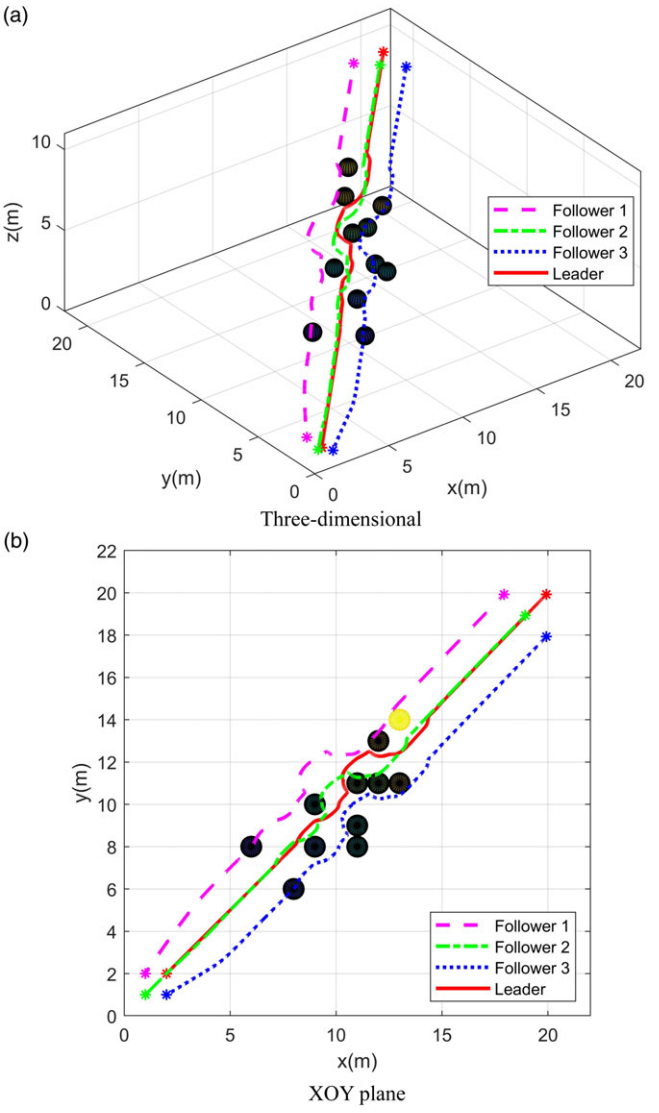

Figure 8. *Formation consensus of four QUAVs.*

In order to realise the QUAV formation to maintain formation and avoid obstacles autonomously, adaptive inter-QUAV communication weights are considered in this paper. Add a weight to the algorithm $\omega_{ij}(t)$ that varies with the position of QUAV i and QUAV j, and the system reaches state consensus when $\|x_i(t) - x_j(t)\| \to 0$. The designed multi-QUAVs finite-time consensus obstacle avoidance protocol is

https://doi.org/10.1017/aer.2024.115 Published online by Cambridge University Press

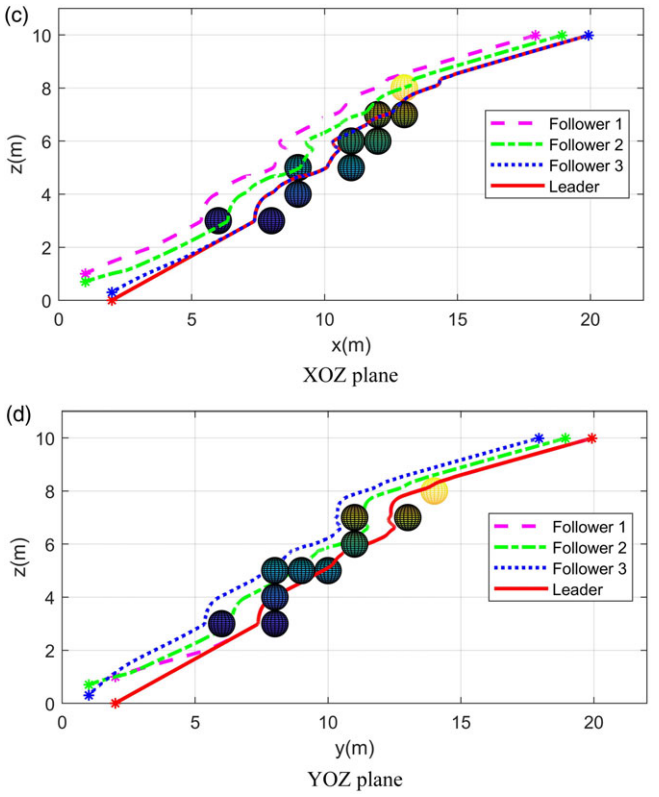

Figure 8. *(Continued)*

shown in Equation (26):

$$u_i(t) = \omega_{ij}(t)[\sum_{j\in N_i} a_{ij} sig(x_j(t-\tau) - x_i(t-\tau))^{\alpha} + a_{i0} sig(x_0(t-\tau) - x_i(t-\tau))^{\alpha} + \gamma \sum_{j\in N_i} a_{ij}(x_j(t-\tau) - x_i(t-\tau)) + \gamma a_{i0}(x_0(t-\tau) - x_i(t-\tau))] + F_i(t) \tag{26}$$

where $\omega_{ij}(t) = 2 - e^{-(x_j(t-\tau)-x_i(t-\tau))^2}$, $F_i(t)$ denotes the combined force of the artificial potential field on the QUAV i at moment t.

7.0 Numerical simulation

The effectiveness of the algorithm in an environment without obstacles is verified by MATLAB simulation. QUAVs have a safety radius of $R_S = 0.25$m and a communication radius of $R_C = 3.5$m, and the safety radius between two QUAVs is $R = 2 \times R_S = 0.5$m. The desired positions in Table 1 indicate the position of each QUAV in the desired formation. Based on the position of the leader as a reference, the followers move towards the desired position to form the desired formation.

Each QUAV quickly forms the desired formation under the control of the finite-time consensus protocol. The leader autonomously plans the flight trajectory, and the followers maintain the desired formation and follow the movement of the leader under the control of the consensus agreement. The simulation results of QUAV formation consensus are shown in Fig. 7.

Then, the effectiveness of the algorithm(26) is verified by MATLAB simulation, and both the network topology and the desired formation of the QUAV formation are shown in Fig. 4. The radius of the spherical obstacle $R_O = 0.25$m. The safe radius between the QUAV and the obstacle

https://doi.org/10.1017/aer.2024.115 Published online by Cambridge University Press

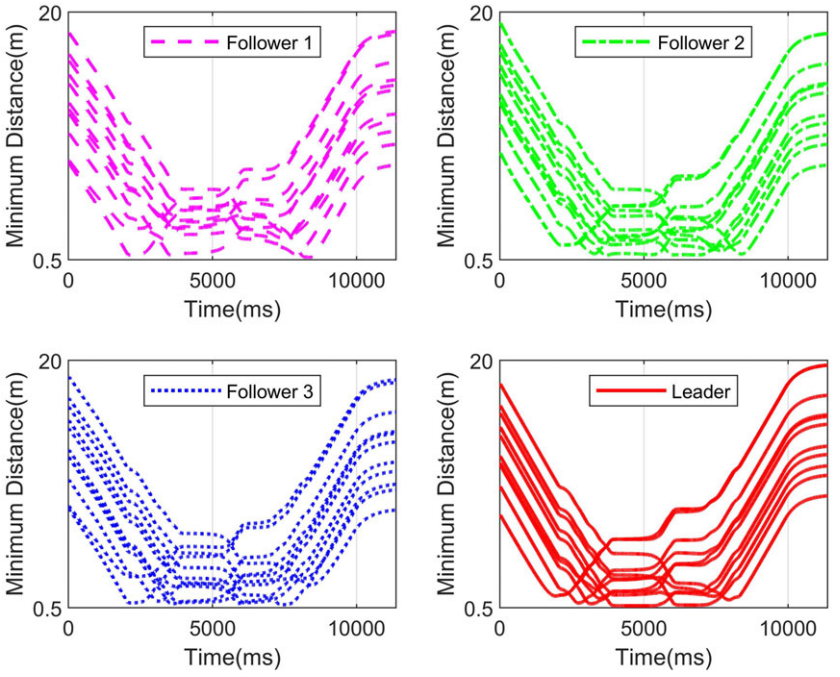

Figure 9. *Distance of multi-QUAVs from obstacles.*

$R = R_O + R_S = 0.5$m. The attraction gain coefficient $K_{att} = 2$, repulsion gain coefficient $K_{rep} = 0.0002$, target influence distance threshold $d_0 = 2$m, maximum obstacle influence distance $d_{\max} = 1$m, and the coordinates of the target point are (20, 20, 10). Several spherical obstacles are randomly generated on the flight trajectory of QUAV formation, with the spherical centre coordinates are (683), (863), (984), (9105), (1185), (1195), (11116), (12116), (12137), (13117), (13148). Maximum velocity constraint is $v_{x\max} = v_{y\max} = v_{z\max} = 3$m/s, $v_{\max} = 3\sqrt{3}$m/s, acceleration $a_x = a_y = a_z = 1\text{m/s}^2$. The sampling time is $\Delta t = 1$ms, time delay $\tau = 10$ms, finite-time coefficient $\alpha = 0.5$, finite-time coefficient $\gamma = 4$. The initial and desired position coordinates of each UAV are shown in Table 2.

The algorithm requires that multi-QUAVs to quickly assemble to form a desired formation, and the QUAV formation should avoid obstacles in the airspace and reach the target position while maintaining the desired formation. The simulation results are shown in Fig. 8. The spherical shape in Fig. 8 represents an obstacle, and its radius is equal to the sum of the actual radius of the obstacle and the safety radius. Multi-QUAVs fly to the target position under the guidance of the leader, and the end of the mission is signaled when the leader reaches the target position. From the four angles of Fig. 8, it can be clearly seen that the multi-QUAVs can quickly assemble to form the desired formation. The QUAV formation can autonomously avoid obstacles while flying to the target position, and the formation is well maintained.

Figure 9 shows the distance between the QUAVs and the obstacles. Observe the minimum value of the Y-axis in the figure. If it is greater than the total radius of the obstacle, it indicates that there is no collision with the obstacle. The distance between the centres of the 4 QUAVs and the centres of the 11 obstacles is always greater than 0.5m, indicating that each QUAV can avoid obstacles.

Figure 10 shows a comparative simulation of QUAV formation consistency obstacle avoidance under the action of traditional artificial potential field method, with the same other conditions. The results indicate that multi-QUAVs cannot maintain the desired formation during obstacle avoidance, demonstrating the effectiveness of the algorithm proposed in this paper.

Figure 11 shows the adjacent distance between any two QUAVs, where D_{12} denotes the distance between follower 1 and follower 2; D_{10} denotes the distance between follower 1 and the leader, and so

https://doi.org/10.1017/aer.2024.115 Published online by Cambridge University Press

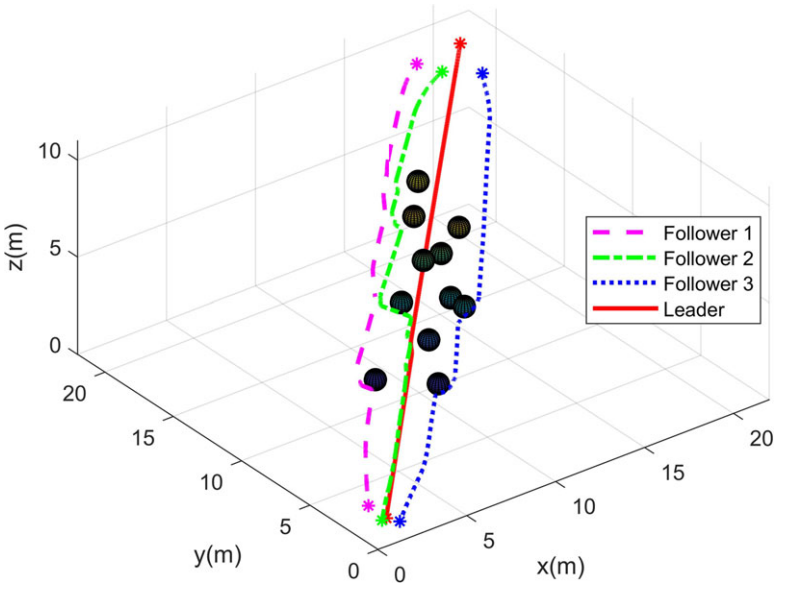

Figure 10. *Comparison of QUAV formation consistency obstacle avoidance.*

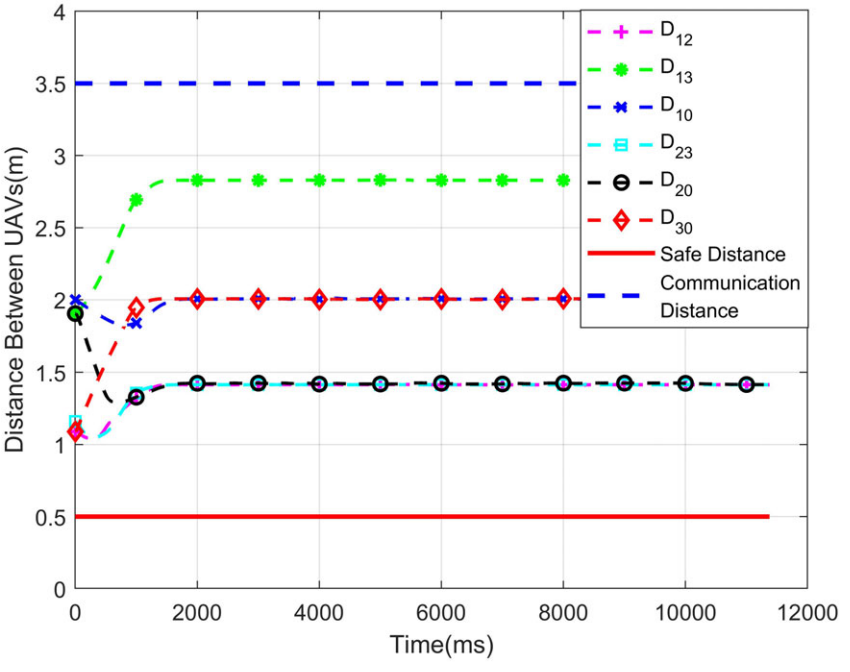

Figure 11. *Position error of multi-QUAVs.*

on. The distance between any two QUAVs is greater than the safe radius and less than the communication radius. This indicates that QUAVs do not collide with each other and are always able to establish communication. After about 1.6s, the distance between any two QUAVs remains unchanged, indicating that the formation is well maintained.

https://doi.org/10.1017/aer.2024.115 Published online by Cambridge University Press

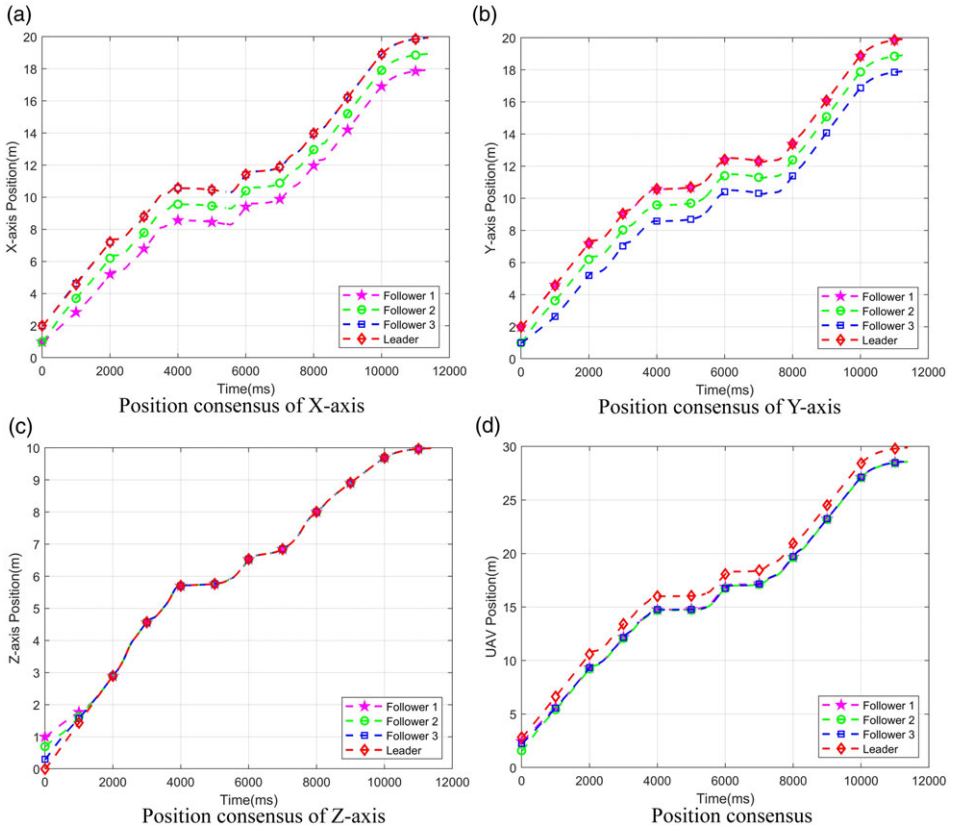

Figure 12. *Position consensus of multi-QUAVs.*

To reflect the QUAV formation consensus motion under this algorithm more clearly, the convergence of the formation's positions on X-axis, Y-axis and Z-axis are simulated by MATLAB. The simulation results are shown in Fig. 12. The leader arrives at the target position at about 11.3s. From Fig. 12(c), it can be seen that the multi-QUAVs complete desired formation at about 1.6s, and the heights of each QUAV on the Z-axis are always synchronised during the subsequent flight.

Simulation of position error curves of each follower and leader, the spacing between the follower and the leader in the desired formation on the axis is $\Delta x = [-2, -1, 0, 0]$, $\Delta y = [0, -1, -2, 0]$, $\Delta z = [0, 0, 0, 0]$, respectively, and the QUAV position error $\Delta = [-2, -\sqrt{2}, -2, 0]$. In Fig. 13, the position error of each follower and leader is the same as the predetermined position, which indicates that the multi-QUAVs can form and maintain the desired formation.

Figure 14 shows a simulation comparison of the Z-axis position error without trajectory segmentation strategy and improved finite-time consensus control, with the same other conditions. The Z-axis position error are selected for comparison, as the positions of each QUAV in the required formation are different on the X-axis and Y-axis, while and the required heights for the Z-axis are the same, but the initial heights are different. The multi-QUAVs can only form the desired formation at about 8s, and the leader reaches the target position at about 12.3s. It is verified that the multi-QUAV finite-time consensus protocol enables multi-QUAVs to quickly assemble to form a desired formation, and the trajectory segmentation strategy can improve task execution efficiency.

Figure 15(a)–(c) show the velocity components of the QUAVs with the maximum constraint of 3m/s, and Fig. 15(d) shows the velocity of the QUAVs with the maximum constraint of $3\sqrt{3}$m/s. None of the

https://doi.org/10.1017/aer.2024.115 Published online by Cambridge University Press

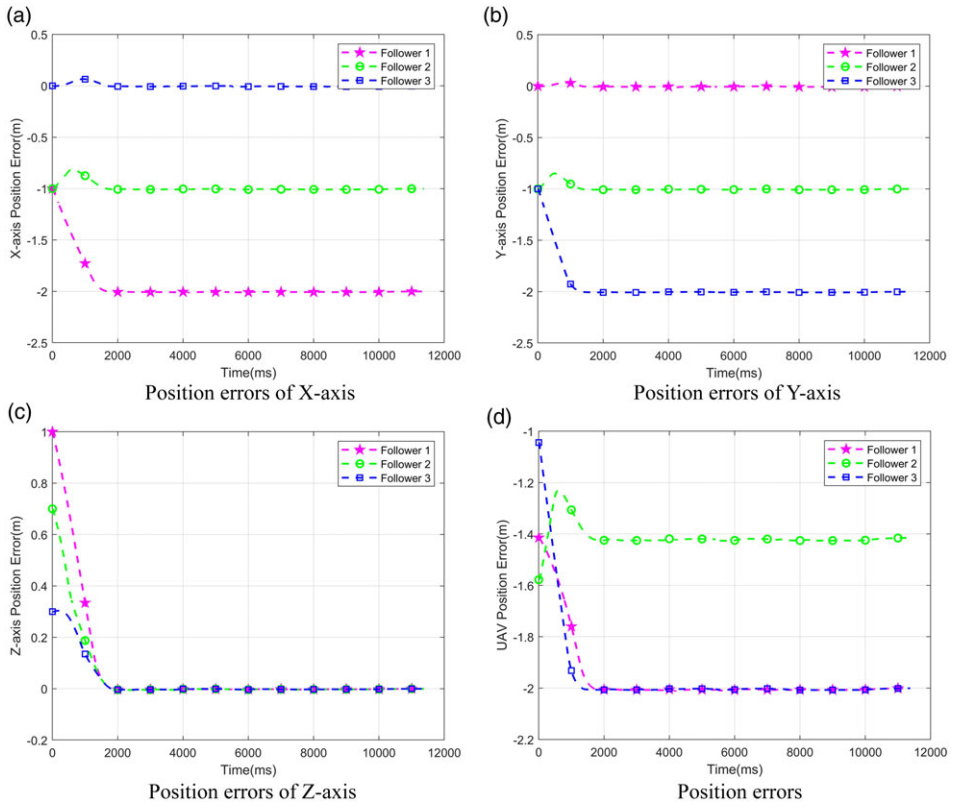

Figure 13. *Positional errors of leader and followers.*

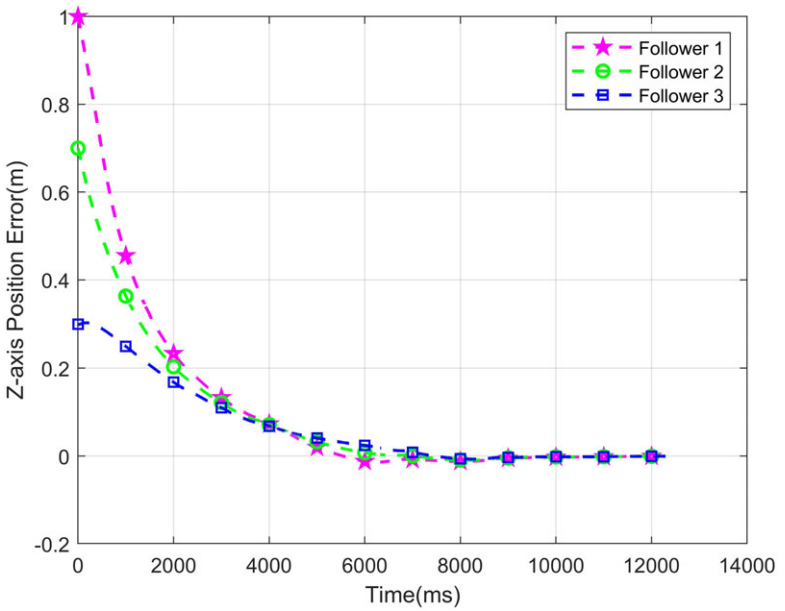

Figure 14. *Comparison of position errors of Z-axis.*

https://doi.org/10.1017/aer.2024.115 Published online by Cambridge University Press

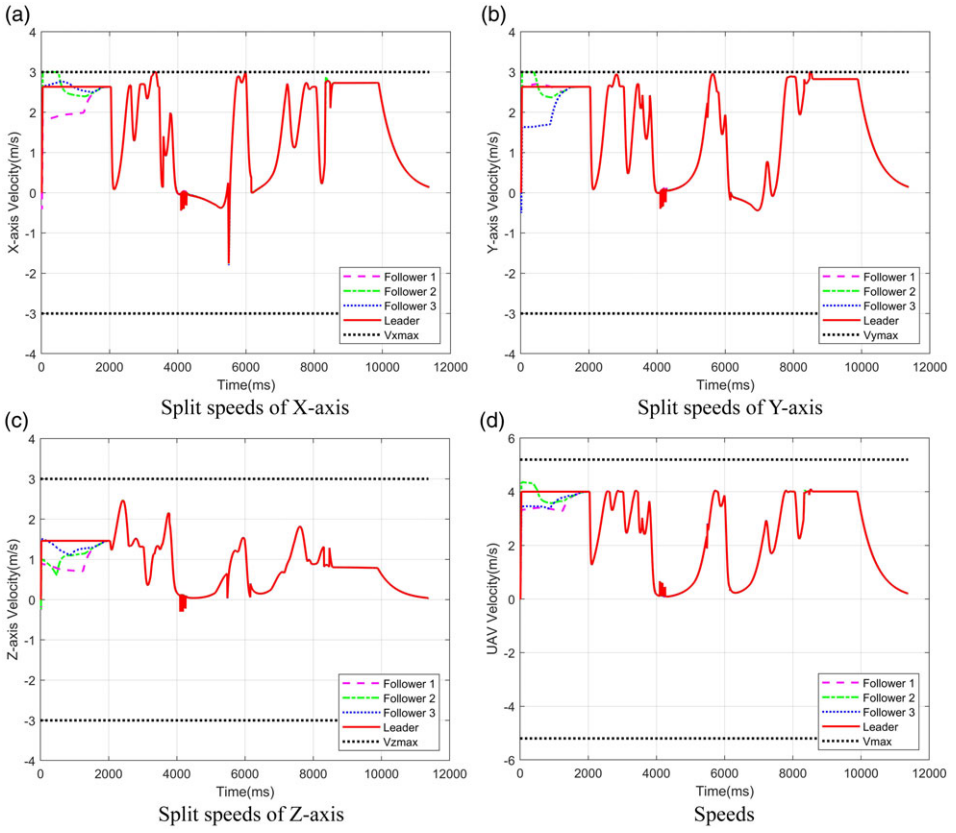

Figure 15. *Speeds of multi-QUAVs.*

QUAVs exceeded the maximum velocity constraint and converged uniformly in approximately 1.6s. Afterwards, each QUAV has the same speed, indicating that the formation is well maintained.

8.0 Conclusion

A finite time consensus obstacle avoidance algorithm for QUAV formation with time delay was designed by combining an improved finite time consensus protocol with an improved artificial potential field method. The multi-QUAVs can be quickly assembled to form the desired formation through the improved finite-time consensus protocol. Under the improved artificial potential field method, the QUAV formation flies towards the target position and avoids obstacles. The trajectory segmentation strategy reduces the complexity of obstacle avoidance environments. The effectiveness of the proposed method is verified by MATLAB simulation. The state convergence time for multi-QUAVs is much faster than the traditional finite-time consensus control method. QUAV formation can successfully avoid obstacles and reach the target position faster than without trajectory segmentation strategy. Multi-QUAVs can form the desired formation and fly to the target position faster, maintain the formation during obstacle avoidance and improve task execution efficiency.

Acknowledgements. This work was supported by the National Natural Science Foundation of China (61976237, 62103456), the Science and Technology Innovation Team of Colleges and Universities in Henan Province (22IRTSTHN015), the Central Plains Thousand Talents Plan Top Talents in Central Plains (ZYQR201810162), the Natural Science Foundation of Henan Province (202300410511), the Key R&D and Promotion Projects (tackling of key scientific and technical problems) in Henan Province, China (232102111129), the Basic research business fees for provincial undergraduate universities of Zhongyuan University of

https://doi.org/10.1017/aer.2024.115 Published online by Cambridge University Press

Technology, China (K2022YY010), the Key Research and Development Program of Henan (241111210100), Discipline Strength Improvement Plan of Zhongyuan University of Technology, China (SD202210).

Data availability statement. Our manuscript has no associated data.

Competing interests. The authors declare that they have no conflict of interest.

References

[1] Greenwood, W.W., Lynch, J.P. and Zekkos, D. Applications of UAVs in civil infrastructure, *J. Infrastruct. Syst.*, 2019, **25,** (2), p 04019002.
[2] Shakhatreh, H., Sawalmeh, A.H., Al-Fuqaha, A., et al. Unmanned aerial vehicles (UAVs): A survey on civil applications and key research challenges, *IEEE Access*, 2019, **7**, pp 48572–48634.
[3] Kose, O., Oktay, T. and Özen, E. Simultaneous arm morphing quadcopter and autonomous flight system design, *Aircraft Eng. Aerospace Technol.*, 2023, **95,** (10), pp 1624–1632.
[4] Aslan, S, and Oktay, T. Path planning of an unmanned combat aerial vehicle with an extended-treatment-approach-based immune plasma algorithm, *Aerospace*, 2023, **10,** (5), p 487.
[5] Kartal, Y., Subbarao, K., Gans, N.R., et al. Distributed backstepping based control of multiple UAV formation flight subject to time delays, *IET Control Theory Appl.*, 2020, **14,** (12), pp 1628–1638.
[6] Zhihao, C.A.I., Longhong, W., Jiang, Z., et al. Virtual target guidance-based distributed model predictive control for formation control of multiple UAVs, *Chin. J. Aeronaut.*, 2020, **33,** (3), pp 1037–1056.
[7] Aslan, S., Demirci, S., Oktay, T., et al. Percentile-based adaptive immune plasma algorithm and its application to engineering optimization, *Biomimetics*, 2023, **8,** (6), p 486.
[8] Oktay, T. and Eraslan, Y. Autonomous flight performance optimization of fixed-wing unmanned aerial vehicle with morphing wingtip, *Aircraft Eng. Aerospace Technol.*, 2024, **96,** (3), pp 475–482.
[9] Chen, X., Tang, J. and Lao, S. Review of unmanned aerial vehicle swarm communication architectures and routing protocols, *Appl. Sci.*, 2020, **10,** (10), p 3661.
[10] Loria, A., Dasdemir, J. and Jarquin, N.A. Leader–follower formation and tracking control of mobile robots along straight paths, *IEEE Trans. Control Syst. Technol.*, 2015, **24,** (2), pp 727–732.
[11] Garcia-Aunon, P., Del Cerro, J. and Barrientos, A. Behavior-based control for an aerial robotic swarm in surveillance missions, *Sensors*, 2019, **19,** (20), p 4584.
[12] Askari, A., Mortazavi, M. and Talebi, H.A. UAV formation control via the virtual structure approach, *J. Aerospace Eng.*, 2015, **28,** (1), p 04014047.
[13] Yoshioka, C. and Namerikawa, T. Observer-based consensus control strategy for multi-agent system with communication time delay, *2008 IEEE International Conference on Control Applications*, IEEE, 2008, pp 1037–1042.
[14] Jadbabaie, A., Lin, J. and Morse, A.S. Coordination of groups of mobile autonomous agents using nearest neighbor rules, *IEEE Trans. Autom. Control*, 2003, **48,** (6), pp 988–1001.
[15] Vicsek, T., Czirók, A., Ben-Jacob, E., et al. Novel type of phase transition in a system of self-driven particles, *Phys. Rev. Lett.*, 1995, **75,** (6), p 1226.
[16] Olfati-Saber, R. and Murray, R.M. Consensus problems in networks of agents with switching topology and time-delays, *IEEE Trans. Autom. Control*, 2004, **49,** (9), pp 1520–1533.
[17] Ni, W. and Cheng, D. Leader-following consensus of multi-agent systems under fixed and switching topologies, *Syst. Control Lett.*, 2010, **59,** (3-4), 209–217.
[18] Khatib, O. Real-time obstacle avoidance for manipulators and mobile robots, *Int. J. Rob. Res.*, 1986, **5,** (1), pp 90–98.
[19] Lawrence, D., Frew, E. and Pisano, W. Lyapunov vector fields for autonomous UAV flight control, *AIAA Guidance, Navigation and Control Conference and Exhibit*, 2007, p 6317.
[20] Goncalves, V.M., Pimenta, L.C.A., Maia, C.A., et al. Vector fields for robot navigation along time-varying curves in n-dimensions, *IEEE Trans. Robot.*, 2010, 26, (4), pp 647–659.
[21] Wilhelm, J.P. and Clem, G. Vector field UAV guidance for path following and obstacle avoidance with minimal deviation, *J. Guidance Control Dyn.*, 2019, **42,** (8), pp 1848–1856.
[22] Hung, N., Rego, F., Quintas, J., et al. A review of path following control strategies for autonomous robotic vehicles: Theory, simulations, and experiments, *J. Field Robot.*, 2023, **40,** (3), pp 747–779.
[23] Moreau, L. Stability of multiagent systems with time-dependent communication links, *IEEE Trans. Autom. Control*, 2005, **50,** (2), pp 169–182.
[24] Wang, L., Chen, Z., Liu, Z., et al. Finite time agreement protocol design of multi-agent systems with communication delays, *Asian J. Control*, 2009, **11,** (3), pp 281–286.
[25] Abdessameud, A. and Tayebi, A. Formation control of VTOL unmanned aerial vehicles with communication delays, *Automatica*, 2011, **47,** (11), pp 2383–2394.
[26] Sun, F. and Guan, Z.H. Finite-time consensus for leader-following second-order multi-agent system, *Int. J. Syst. Sci.*, 2013, **44,** (4), pp 727–738.
[27] Ma, J., Sun, D., Ji, H., et al. Leader-following consensus of multi-agent systems with limited data rate, *J. Franklin Inst.*, 2017, **354,** (1), pp 184–196.
[28] Shang, Y. Finite-time consensus for multi-agent systems with fixed topologies, *Int. J. Syst. Sci.*, 2012, **43,** (3), pp 499–506.

https://doi.org/10.1017/aer.2024.115 Published online by Cambridge University Press

[29] Liu, R., Qu, B., Wei, T., et al. Research on UAV formation obstacle avoidance based on consistency control, *2023 IEEE 12th Data Driven Control and Learning Systems Conference (DDCLS)*, IEEE, 2023, pp 155–160.
[30] Xiao, Q.Y., Wu, Z.H. and Peng, L. Fast finite-time consensus tracking of first-order multi-agent systems with a virtual leader, *Appl. Mech. Mater.*, 2014, **596**, pp 552–559.
[31] Sun, F.L. and Zhu, W. Finite-time consensus for leader-following multi-agent systems over switching network topologies, *Chin. Phys. B*, 2013, **22,** (11), p 110204.
[32] Zheng, Y., Chen, W. and Wang, L. Finite-time consensus for stochastic multi-agent systems, *Int. J. Control*, 2011, **84,** (10), pp 1644–1652.
[33] Ren, W. and Beard, R.W. Consensus seeking in multiagent systems under dynamically changing interaction topologies, *IEEE Trans. Autom. Control*, 2005, **50,** (5), pp 655–661.
[34] Wang, L. and Xiao, F. Finite-time consensus problems for networks of dynamic agents, *IEEE Trans. Autom. Control*, 2010, **55,** (4), pp 950–955.
[35] Cortés, J. Finite-time convergent gradient flows with applications to network consensus, *Automatica*, 2006, **42,** (11), pp 1993–2000.
[36] Luan, T., Tan, Z., You, B., et al. Path planning of unmanned surface vehicle based on artificial potential field approach considering virtual target points, *Trans. Inst. Meas. Control*, 2023, 01423312231190208.

Cite this article: Zhang L., Liu R., Qu B., Wei T., Chai X. and Yan L. (2025). Research on multiple quadrotor UAV formation obstacle avoidance based on finite-time consensus. *The Aeronautical Journal*, **129**, 939–959. https://doi.org/10.1017/aer.2024.115